Nonadiabatic Strong Field Ionization of Atomic Hydrogen

D. Trabert,[1] N. Anders,[1] S. Brennecke,[2,*] M. S. Schöffler,[1] T. Jahnke,[1] L. Ph. H. Schmidt,[1] M. Kunitski,[1] M. Lein,[2] R. Dörner,[1] and S. Eckart[1,†]

[1]*Institut für Kernphysik, Goethe-Universität, Max-von-Laue-Straße 1, 60438 Frankfurt, Germany*

[2]*Institut für Theoretische Physik, Leibniz Universität Hannover, Appelstraße 2, 30167 Hannover, Germany*

(Received 29 July 2021; accepted 7 December 2021; published 30 December 2021)

We present experimental data on the nonadiabatic strong field ionization of atomic hydrogen using elliptically polarized femtosecond laser pulses at a central wavelength of 390 nm. Our measured results are in very good agreement with a numerical solution of the time-dependent Schrödinger equation (TDSE). Experiment and TDSE show four above-threshold ionization peaks in the electron's energy spectrum. The most probable emission angle (also known as "attoclock offset angle" or "streaking angle") is found to increase with energy, a trend that is opposite to standard predictions based on Coulomb interaction with the ion. We show that this increase of deflection angle can be explained by a model that includes nonadiabatic corrections of the initial momentum distribution at the tunnel exit and nonadiabatic corrections of the tunnel exit position itself.

DOI: 10.1103/PhysRevLett.127.273201

Atomic hydrogen is the simplest atomic system and thus it is often used to benchmark theoretical models, making it the drosophila of theories of light-matter interaction. Its key advantage is the absence of multielectron effects and the well-defined electrostatic potential of the proton, eliminating the need for approximations. While atomic hydrogen is very frequently used in theoretical studies and textbook examples, due to the experimental challenges connected with producing hydrogen atoms in an ultrahigh vacuum environment and separating events from those resulting from nondissociated H_2, only a single experiment has been reported for strong field ionization [1]. In this pioneering work, Sainadh *et al.* have applied the technique of angular streaking [2,3] to adiabatic tunnel ionization of atomic hydrogen. In angular streaking experiments, the most probable electron emission angle is analyzed and the experimentally obtained results are used to benchmark theoretical models to better understand strong field ionization [4–10].

In this Letter, we report on a similar experiment to the one by Sainadh *et al.* [1], but target nonadiabatic strong field ionization [11–14], instead of the much better understood adiabatic process [15]. Technically this is done by choosing a different intensity and wavelength regime as in [1]. For adiabatic tunnel ionization, the experimentally measured electron energy spectrum usually shows only one broad peak. We observe four above-threshold ionization (ATI) peaks [16,17] in the electron's energy spectrum that are spaced by the photon energy, which allows for the investigation of angular streaking for each energy peak separately [18,19]. To this end, atomic hydrogen is irradiated with an elliptically polarized femtosecond laser pulse at a central wavelength of 390 nm and a peak intensity of 1.4×10^{14} W/cm^2. This corresponds to a Keldysh parameter of 3, indicating that the temporal evolution of the tunnel barrier cannot be neglected under these conditions and that field-driven dynamics before and during tunneling will contribute to the ionization dynamics [11].

In our experiment, atomic hydrogen was generated using a commercially available source (H-flux, Tectra GmbH). Hydrogen gas is thermally dissociated in a tungsten capillary heated by electron bombardment. The hydrogen beam is collimated to a half opening angle of about 1° using an aperture and reaches the laser focus after propagating in vacuum for 260 mm. Our optical setup is based on a commercial Ti:sapphire femtosecond laser system (100 kHz, Wyvern-500, KMLabs). We used a 200 μm β-barium-borate crystal to frequency double the laser pulses. The power was adjusted by a $\lambda/2$ wave plate and a subsequent thin-film polarizer. The polarization of the laser pulses was controlled using a $\lambda/4$ wave plate followed by a $\lambda/2$ wave plate. We use elliptically polarized light with an ellipticity of $\epsilon = 0.85$. The duration of the laser pulses at a central wavelength of 390 nm was 50 fs, and the pulses were focused by a spherical mirror ($f = 60$ mm) onto the jet of hydrogen atoms. A COLTRIMS reaction microscope [20] was used to measure the three-dimensional momenta of electron and ion in coincidence. In the spectrometer, a homogeneous electric field of 27 V/cm and a parallel homogeneous magnetic field of 14.2 G separated and accelerated the charged particles toward two position- and time-sensitive detectors [21]. The length of the ion (electron) spectrometer was 17 cm (31 cm). Each detector comprises a stack of two microchannel plates with a diameter of 80 mm followed by a hexagonal delay line anode. The time-of-flight and position-of-impact

information were used to calculate the momenta of electron and ion, which were measured in coincidence. The absolute orientation of the polarization ellipse in the experiment has been determined by the most probable emission angle of H^+ ions resulting from the reaction $H_2 \rightarrow H + H^+ + e^-$ undergone by H_2 molecules [22] that were not dissociated in the atomic hydrogen source. The H^+ ions from ionization of atomic hydrogen and those from ionization of H_2 with subsequent dissociation are unambiguously distinguishable, as the latter carry a momentum of about 9 a.u. The average intensity in the focus was 9×10^{13} W/cm^2 (taking volume averaging into account as in Ref. [23]). This corresponds to a peak intensity of 1.4×10^{14} W/cm^2 (peak electric field of $E_{\text{peak}} = 0.046$ a.u. at an ellipticity of $\epsilon = 0.85$). The calibration of the laser intensity was done by comparing the measured electron energy distribution to numerical solutions of the time-dependent Schrödinger equation (TDSE). The numerical solutions of the TDSE are found in three dimensions in the length gauge for a laser pulse with a $\sin^2$ envelope and a duration of 20 optical cycles. The numerical propagation uses the pseudospectral method described in Refs. [24–26]. In order to obtain photoelectron momentum distributions, we project the final electronic wave function on the exact scattering states of the Coulomb potential. Afterward, the distributions are averaged over four carrier-envelope phase values from 0 to 2π and over the focal volume intensity distribution, assuming a Gaussian beam profile in the focus. We have confirmed that the observables presented in this Letter do not significantly depend on the pulse length that is used in the TDSE simulation by varying the pulse length in the range of 10–30 optical cycles.

Figure 1(a) shows the electron momentum distribution projected onto the laser's polarization plane ($p_x p_y$ plane). Four ATI rings are visible that are spaced by the photon energy of 3.18 eV. The orientation of the major axis of the polarization ellipse is aligned along the p_x direction. Figure 1(b) shows the corresponding result that is obtained from a numerical solution of the TDSE. Experiment and the TDSE result show excellent agreement. This is underlined by Fig. 1(c), which shows the corresponding electron energy distributions that are also in good agreement.

In order to compare the angular offset angles α_{off}, the momentum distributions from Figs. 1(a) and 1(b) are shown in Figs. 2(a) and 2(b) in cylindrical coordinates. α_{off} is the angle between the observed angle of maximum electron yield and the minor axis of the polarization ellipse (see Fig. 1). Rowwise normalization is performed to improve the visibility of the angular distributions for less probable p_r. In addition to the good agreement of experiment and the TDSE, it is evident that α_{off} increases as a function of the radial momentum in the laser's polarization plane $p_r = \sqrt{p_x^2 + p_y^2}$. What is the microscopic reason for this dependence of α_{off} on p_r?

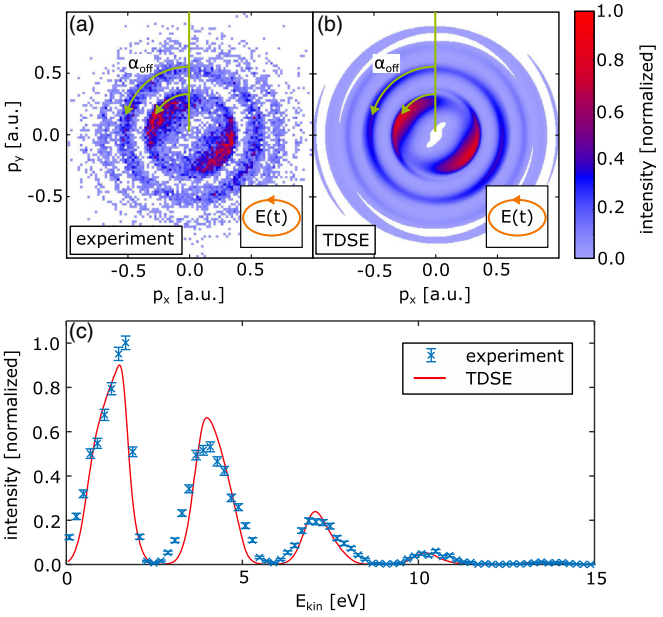

FIG. 1. (a) Measured electron momentum distribution projected onto the laser's polarization plane for the ionization of atomic hydrogen by femtosecond laser pulses at a central wavelength of 390 nm, an ellipticity of $\epsilon = 0.85$, and a peak intensity of 1.4×10^{14} W/cm^2. The light's helicity and the orientation of the polarization ellipse are indicated by the inset in the lower right corner. (b) Focal-averaged numerical solution of the TDSE for the parameters that were used in (a). α_{off} indicates the "angular offset" with respect to the minor axis of the ellipse of the laser electric field and the negative vector potential in (a) and (b). The intensity in (a) [(b)] has been normalized to a maximum of 1 [0.8]. (c) shows a comparison of the electron energy distribution for the data shown in (a) and (b). The error bars show statistical errors only.

A common way to model strong field ionization in a time-dependent electric field $\vec{E}(t)$ is to split the ionization dynamics into two steps [27]. First, at a given instant t_0 the electron tunnels through the time-dependent potential barrier that is formed by the ionic potential and the laser electric field. The electron is released with an initial momentum $\vec{p}_{\text{init}}$ at a position $\vec{r}_0$ that is antiparallel to the electric field vector $\vec{E}(t_0)$ at the time t_0. It is typically assumed that $\vec{p}_{\text{init}}$ is perpendicular to $\vec{E}(t_0)$ [18,28]. In the second step, the classical forces that act upon the electron and are due to the laser field and Coulomb interaction with the ion determine the electron's dynamics. For elliptically polarized light, the probability for tunneling maximizes at the two instants per laser cycle when the electric field vector points along the major axis of the polarization ellipse. Those instants in time are t_1 and $t_2 = t_1 + T/2$, where T is the duration of one cycle of the light field. $\vec{p}_{\text{init}}$ is usually small and is typically modeled by a nearly Gaussian distribution [29]. Therefore, if Coulomb interaction after tunneling is neglected, this two-step model yields maximum probability for the occurrence of momenta of

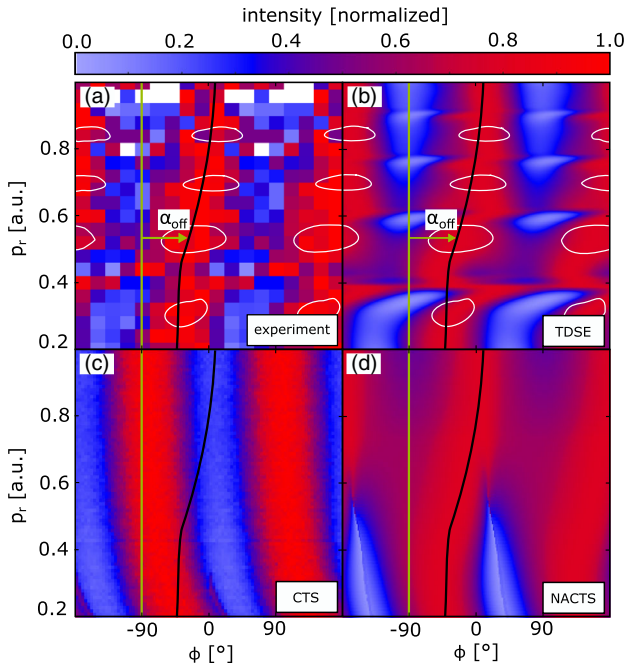

FIG. 2. (a) [(b)] shows the electron momentum distribution from Fig. 1(a) [Fig. 1(b)] in cylindrical coordinates ($p_r = \sqrt{p_x^2 + p_y^2}$ and ϕ is the angle of $\vec{p}_{\mathrm{elec}}$ in the laser polarization plane) after rowwise normalization. α_{off} indicates the angular offset, the white contours indicate the ATI peak positions. (c) The rowwise normalized electron momentum distribution that is obtained from the CTS model with initial momenta distributed according to ADK theory, taking Coulomb interaction after tunneling into account and using the tunnel exit position from the TIPIS model in analogy to (a) and (b). (d) The result from our NACTS model. Within the NACTS model, the ionization probability and the initial conditions are taken from SFA. The black line guides the eye and is the same in all panels. The data in (a)–(d) have been symmetrized making use of the twofold symmetry. Every row has been normalized independently. The intensity in (a) [(b)–(d)] has been normalized to a maximum of 1 [0.8].

$\vec{p}_{\mathrm{elec}} = -\vec{A}(t_1)$ and $\vec{p}_{\mathrm{elec}} = -\vec{A}(t_2)$ giving rise to a twofold symmetry of the electron momentum distribution in the plane of polarization. The orientation of this twofold symmetric distribution in the plane of polarization is the basis of "attoclock experiments" [3–9]. The deviation of the orientation of the twofold symmetric distribution with respect to the direction that is defined by $-\vec{A}(t_1)$ and $-\vec{A}(t_2)$ is referred to as angular offset [30]. A state-of-the-art classical model is the semiclassical two-step (SCTS) model that includes Coulomb interaction after tunneling and even allows for the modeling of interference [27,28,31,32].

In the remainder of this Letter, we build on the classical two-step (CTS) model [14], which is equivalent to the SCTS model [28] but neglects interference. As a reference, we first perform a CTS simulation in which the tunneling probability is given by the Ammosov-Delone-Krainov (ADK) theory [15,28]. This is the CTS model, which is often used to model attoclock experiments [9,33,34]. It takes Coulomb interaction after tunneling into account and uses the tunnel exit position from the TIPIS model (tunnel ionization in parabolic coordinates with induced dipole and Stark shift). In the following, we neglect the polarizability of the hydrogen atom. Inclusion of the polarizability would lead to a Stark shift of the ionization potential by about 0.13 eV. Within the TIPIS model, the tunnel exit position is given by

$$r_{\mathrm{TIPIS}}[\vec{E}(t)] = \frac{I_p + \sqrt{I_p^2 - (4 - \sqrt{8I_p})|\vec{E}(t)|}}{2|\vec{E}(t)|} \quad (1)$$

Here, $I_p = 0.5$ a.u. is the ionization potential of atomic hydrogen. The tunnel exit position r_{TIPIS} depends solely on the magnitude of the instantaneous laser electric field $|\vec{E}(t)|$ which makes TIPIS an adiabatic model. The result from this CTS simulation is shown in Fig. 2(c). As expected, the Coulomb potential leads to a nonzero offset angle, but the effect decreases with increasing p_r; a trend just opposite to the findings obtained from experiment and TDSE.

In a next step, we employ a hybrid model that combines the strength of strong field approximation (SFA), which is the inclusion of nonadiabatic dynamics in the classically forbidden region (also referred to as tunnel), and the strength of the CTS model, which is the inclusion of Coulomb interaction after the electron is released from the classically forbidden region. We refer to this improved CTS model as the nonadiabatic, classical two-step model (NACTS). The NACTS model and the CTS model are both based on classical trajectories. In contrast to the CTS model, the NACTS model uses the initial probability distribution from SFA in order to launch a swarm of classical trajectories. This implies that the momenta along the direction of the electric field at the instant of ionization can be nonzero, which is an important difference with respect to ADK theory. The same holds true for the initial position of the classical trajectories within the NACTS model, which are not simply calculated using the TIPIS model, but are also obtained from a SFA simulation [35,36]. In summary, our NACTS simulations are equivalent to the scheme presented in Ref. [37], except that interference of trajectories is neglected. The NACTS model results in the distribution that is shown in Fig. 2(d). Its exact shape is affected by the correlated initial momentum and position distribution (see Supplemental Material [38] for details). The result from the NACTS model shows the same trend as observed in the experiment and the TDSE simulation. Comparing the two different classical models [Figs. 2(c) and 2(d)], it is found that the result from the NACTS model shows superior agreement with the experiment and with the result from the TDSE simulation. It

should be noted that the conclusions that are drawn from the CTS and the NACTS model are limited by the validity of the models (see Supplemental Material [38] for details). Within the CTS model there is an adiabatic tunneling step that is modeled by ADK theory. This is in contrast to SFA, which is the basis for the NACTS model. SFA also works for $\gamma > 1$ and makes no assumption on the existence of tunneling in the sense of a slowly varying potential barrier.

To quantitatively compare the results shown in Fig. 2, we extract the angular offset for each ATI peak in Figs. 2(a) and 2(b). To this end, we integrate the signal corresponding to each ATI peak separately and thereby obtain an angular distribution for each ATI peak. Then, we determine the offset angle α_{off} from the second-order Fourier coefficients. For the distributions in Figs. 2(c) and 2(d), α_{off} is determined for each row separately. The results are shown in Fig. 3(a) as a function of p_r. This quantitative comparison underlines the excellent agreement of the TDSE simulation with the experiment. Further, it is evident that the NACTS model qualitatively agrees with the experiment and the result from the TDSE simulation. To summarize the importance of the dependence of the initial position on the initial momentum, Fig. 3(b) compares $\vec{r}_{\mathrm{TIPIS}}$ and $\vec{r}_{\mathrm{SFA}}$ for tunneling at the peak electric field of an elliptically polarized light field at 390 nm with a peak electric field of 0.046 a.u. and an ellipticity of 0.85.

The physics behind the dependence of the initial position on the initial momentum is intriguingly simple: For nonadiabatic tunneling, the energy at the tunnel exit can be higher than the ground state energy because energy can be absorbed from the light field in the classically forbidden region [11]. Klaiber *et al.* have shown that nonadiabatic tunneling can be modeled as nonresonant multiphoton excitation and subsequent adiabatic tunneling [13,41]. Within this picture, the absorption of energy from the light field leads to an inward shift of the tunnel exit position as illustrated in Fig. 3(c), since it effectively reduces I_p in Eq. (1) by the energy that is absorbed from the light field. For almost circularly polarized light, the absorption of energy from the light field also induces a well-defined change in angular momentum. This results in an increased initial momentum at the tunnel exit [14] and explains the overall decrease of $\vec{r}_{\mathrm{SFA}}$ as a function of $p_\perp$. Interestingly, for very high $p_\perp$ the energy $\frac{1}{2}p_\perp^2$ is not negligible compared to I_p, which manifests as an effectively increased I_p, which explains the increasing values of $\vec{r}_{\mathrm{SFA}}$ for $p_\perp > 0.7$ a.u.

Figure 3(c) visualizes that SFA does not include any long-range potential of the ion. Neglecting Coulomb effects on the under-the-barrier dynamics is a possible reason why the result from our NACTS model [see Fig. 2(d)] does not show complete agreement with the experiment. Further, we observe that the TDSE simulation shows a dependence of α_{off} on p_r even within single ATI peaks, as can be seen in Fig. 2(b). Interestingly, such a feature is also seen in the experiment at $p_r \approx 0.4$ a.u. [see Fig. 2(a)]. Currently, we

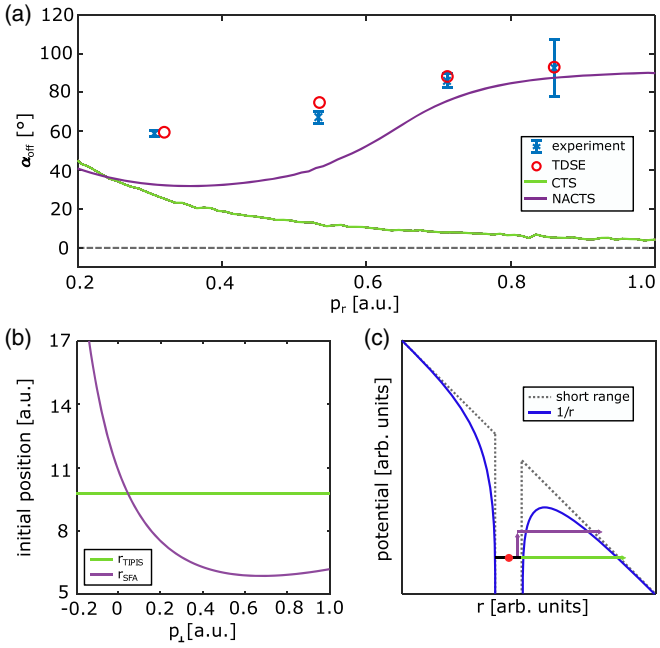

FIG. 3. (a) The angular offset α_{off} is plotted as a function of the radial momentum p_r for the data from Figs. 2(a)–2(d). Error bars show statistical errors only. The gray dashed line guides the eye and shows the emission angle of electrons that tunnel at the peak electric field without taking Coulomb interaction into account. The magnitude of the negative vector potential at the peak of the laser pulse is 0.33 a.u. (b) Illustrates that the tunnel exit position within the TIPIS model does not depend on the initial momentum at the tunnel exit $p_\perp$. SFA predicts decreasing values for the initial position $\vec{r}_{\mathrm{SFA}}$ as a function of $p_\perp$ for $0 < p_\perp < 0.7$ a.u. The most probable value of $p_\perp$ from SFA is 0.15 a.u. (c) Visualization of a potential microscopic explanation for the dependence of $\vec{r}_{\mathrm{SFA}}$ on $p_\perp$ (see text).

cannot explain this observation, which warrants further research. We speculate that this might be related to focal averaging, as we observe an offset angle for the lowest energy peak of only 50° in the TDSE simulation without volume averaging for an intensity of 9×10^{13} W/cm^2.

In conclusion, we have presented a benchmark experiment on the nonadiabatic strong field ionization of atomic hydrogen. The result is in excellent agreement with our *ab initio* TDSE simulation. The simplicity of the structure of atomic hydrogen allows for the exclusion of multielectron effects as well as initial states with atomic orbitals carrying angular momentum [42]. We find that the CTS model, which is typically used to interpret attoclock experiments, is not able to describe the angular offset α_{off} as a function of the electron momentum in the plane of polarization p_r. We find that our NACTS model, a semiclassical model with nonadiabatic initial conditions and ionization probabilities from SFA, reproduces the experimental findings qualitatively. Within the NACTS model, the initial momenta and the initial positions of the wave packet at the tunnel exit are correlated, leading to a clearly

improved agreement with the experiment. TDSE calculations over a wide range of Keldysh parameters (see Supplemental Material [38]) suggest that the nonadiabatic effects discussed in this Letter significantly alter the offset angle for $\gamma > 0.5$. The inclusion of nonadiabatic effects, as in our NACTS model, can extend the validity range of two-step models to $\gamma \approx 3$, which is considered outside the tunneling regime in the usual strong field terminology. This allows for a new class of attoclock experiments that are resolved with respect to the electrons radial momentum. We expect that the NACTS model will help to interpret future attoclock experiments and will thereby lead to a better understanding of the role of electron positions and momenta in the ionization process. The NACTS model is an important step toward probing the wave packets tunnel exit position with subangstrom precision [43] as proposed by Kheifets [44] who has referred to this approach as "nanoruler." We expect that our findings will serve as a benchmark for the development of models for other atoms and small (chiral) molecules.

The experimental work was supported by the DFG (German Research Foundation). S. B. acknowledges funding of the German Academic Exchange Service. D. T., M. L., and S. E. acknowledge funding of the DFG through Priority Programme SPP 1840 QUTIF.

*simon.brennecke@itp.uni-hannover.de
†eckart@atom.uni-frankfurt.de

[1] U. S. Sainadh, H. Xu, X. Wang, A. Atia-Tul-Noor, W. C. Wallace, N. Douguet, A. Bray, I. Ivanov, K. Bartschat, A. Kheifets, R. T. Sang, and I. V. Litvinyuk, Attosecond angular streaking and tunnelling time in atomic hydrogen, Nature (London) **568**, 75 (2019).

[2] M. Smolarski, P. Eckle, U. Keller, and R. Dörner, Semiclassical model for attosecond angular streaking, Opt. Express **18**, 17640 (2010).

[3] P. Eckle, A. N. Pfeiffer, C. Cirelli, A. Staudte, R. Dörner, H. G. Muller, M. Büttiker, and U. Keller, Attosecond ionization and tunneling delay time measurements in helium, Science **322**, 1525 (2008).

[4] L. Torlina, F. Morales, J. Kaushal, I. Ivanov, A. Kheifets, A. Zielinski, A. Scrinzi, H. G. Muller, S. Sukiasyan, M. Ivanov, and O. Smirnova, Interpreting attoclock measurements of tunnelling times, Nat. Phys. **11**, 503 (2015).

[5] D. Shafir, H. Soifer, B. D. Bruner, M. Dagan, Y. Mairesse, S. Patchkovskii, M. Ivanov, O. Smirnova, and N. Dudovich, Resolving the time when an electron exits a tunnelling barrier, Nature (London) **485**, 343 (2012).

[6] A. W. Bray, S. Eckart, and A. S. Kheifets, Keldysh-Rutherford Model for the Attoclock, Phys. Rev. Lett. **121**, 123201 (2018).

[7] H. Ni, U. Saalmann, and J.-M. Rost, Tunneling Ionization Time Resolved by Backpropagation, Phys. Rev. Lett. **117**, 023002 (2016).

[8] N. Camus, E. Yakaboylu, L. Fechner, M. Klaiber, M. Laux, Y. Mi, K. Z. Hatsagortsyan, T. Pfeifer, C. H. Keitel, and R. Moshammer, Experimental Evidence for Quantum Tunneling Time, Phys. Rev. Lett. **119**, 023201 (2017).

[9] H. Ni, U. Saalmann, and J.-M. Rost, Tunneling exit characteristics from classical backpropagation of an ionized electron wave packet, Phys. Rev. A **97**, 013426 (2018).

[10] C. Hofmann, A. S. Landsman, and U. Keller, Attoclock revisited on electron tunnelling time, J. Mod. Opt. **66**, 1052 (2019).

[11] M. Yu. Ivanov, M. Spanner, and O. Smirnova, Anatomy of strong field ionization, J. Mod. Opt. **52**, 165 (2005).

[12] I. Barth and O. Smirnova, Nonadiabatic tunneling in circularly polarized laser fields: Physical picture and calculations, Phys. Rev. A **84**, 063415 (2011).

[13] M. Klaiber and J. S. Briggs, Crossover from tunneling to multiphoton ionization of atoms, Phys. Rev. A **94**, 053405 (2016).

[14] S. Eckart, K. Fehre, N. Eicke, A. Hartung, J. Rist, D. Trabert, N. Strenger, A. Pier, L. Ph. H. Schmidt, T. Jahnke, M. S. Schöffler, M. Lein, M. Kunitski, and R. Dörner, Direct Experimental Access to the Nonadiabatic Initial Momentum Offset upon Tunnel Ionization, Phys. Rev. Lett. **121**, 163202 (2018).

[15] M. V. Ammosov, N. B. Delone, and V. P. Krainov, Tunnel ionization of complex atoms and of atomic ions in an alternating electromagnetic field, Sov. Phys. JETP **64**, 1191 (1986), http://www.jetp.ras.ru/cgi-bin/e/index/e/64/6/p1191?a=list.

[16] G. S. Voronov and N. B. Delone, Many-photon ionization of the xenon atom by ruby laser radiation, Sov. Phys. JETP **23**, 54 (1966), http://www.jetp.ras.ru/cgi-bin/e/index/e/23/1/p54?a=list.

[17] P. Agostini, F. Fabre, G. Mainfray, G. Petite, and N. K. Rahman, Free-Free Transitions Following Six-Photon Ionization of Xenon Atoms, Phys. Rev. Lett. **42**, 1127 (1979).

[18] S. P. Goreslavski, G. G. Paulus, S. V. Popruzhenko, and N. I. Shvetsov-Shilovski, Coulomb Asymmetry in Above-Threshold Ionization, Phys. Rev. Lett. **93**, 233002 (2004).

[19] C. Wang, X. Li, X. Liu, J. Li, S. Zhou, Y. Yang, X. Song, J. Chen, W. Yang, and D. Ding, Decoding electron tunnelling delay time by embracing wave-particle duality, arXiv:2104.06144.

[20] J. Ullrich, R. Moshammer, A. Dorn, R. Dörner, L. Ph. H. Schmidt, and H. Schmidt-Böcking, Recoil-ion and electron momentum spectroscopy: Reaction-microscopes, Rep. Prog. Phys. **66**, 1463 (2003).

[21] O. Jagutzki, A. Cerezo, A. Czasch, R. Dörner, M. Hattas, M. Huang, V. Mergel, U. Spillmann, K. Ullmann-Pfleger, T. Weber, H. Schmidt-Böcking, and G. D. W. Smith, Multiple hit readout of a microchannel plate detector with a three-layer delay-line anode, IEEE Trans. Nucl. Sci. **49**, 2477 (2002).

[22] A. Staudte, S. Patchkovskii, D. Pavičić, H. Akagi, O. Smirnova, D. Zeidler, M. Meckel, D. M. Villeneuve, R. Dörner, M. Y. Ivanov, and P. B. Corkum, Angular Tunneling Ionization Probability of Fixed-in-Space H_2 Molecules in Intense Laser Pulses, Phys. Rev. Lett. **102**, 033004 (2009).

[23] P. Wang, A. M. Sayler, K. D. Carnes, B. D. Esry, and I. Ben-Itzhak, Disentangling the volume effect through intensity-difference spectra: Application to laser-induced dissociation of H_2^+, Opt. Lett. **30**, 664 (2005).

[24] X.-M. Tong and S.-I. Chu, Theoretical study of multiple high-order harmonic generation by intense ultrashort pulsed laser fields: A new generalized pseudospectral time-dependent method, Chem. Phys. **217**, 119 (1997).
[25] M. Murakami, O. Korobkin, and M. Horbatsch, High-harmonic generation from hydrogen atoms driven by two-color mutually orthogonal laser fields, Phys. Rev. A **88**, 063419 (2013).
[26] D. Baykusheva, S. Brennecke, M. Lein, and H. J. Wörner, Signatures of Electronic Structure in Bicircular High-Harmonic Spectroscopy, Phys. Rev. Lett. **119**, 203201 (2017).
[27] T. F. Gallagher, Above-Threshold Ionization in Low-Frequency Limit, Phys. Rev. Lett. **61**, 2304 (1988).
[28] N. I. Shvetsov-Shilovski, M. Lein, L. B. Madsen, E. Räsänen, C. Lemell, J. Burgdörfer, D. G. Arbó, and K. Tőkési, Semiclassical two-step model for strong-field ionization, Phys. Rev. A **94**, 013415 (2016).
[29] L. Arissian, C. Smeenk, F. Turner, C. Trallero, A. V. Sokolov, D. M. Villeneuve, A. Staudte, and P. B. Corkum, Direct Test of Laser Tunneling with Electron Momentum Imaging, Phys. Rev. Lett. **105**, 133002 (2010).
[30] P. Eckle, M. Smolarski, P. Schlup, J. Biegert, A. Staudte, M. Schöffler, H. G. Muller, R. Dörner, and U. Keller, Attosecond angular streaking, Nat. Phys. **4**, 565 (2008).
[31] D. G. Arbó, K. L. Ishikawa, K. Schiessl, E. Persson, and J. Burgdörfer, Intracycle and intercycle interferences in above-threshold ionization: The time grating, Phys. Rev. A **81**, 021403(R) (2010).
[32] S. Eckart, M. Kunitski, I. Ivanov, M. Richter, K. Fehre, A. Hartung, J. Rist, K. Henrichs, D. Trabert, N. Schlott, L. Ph. H. Schmidt, T. Jahnke, M. S. Schöffler, A. Kheifets, and R. Dörner, Subcycle interference upon tunnel ionization by counter-rotating two-color fields, Phys. Rev. A **97**, 041402(R) (2018).
[33] C. Z. Bisgaard and L. B. Madsen, Tunneling ionization of atoms, Am. J. Phys. **72**, 249 (2004).
[34] A. N. Pfeiffer, C. Cirelli, M. Smolarski, D. Dimitrovski, M. Abu-Samha, L. B. Madsen, and U. Keller, Attoclock reveals natural coordinates of the laser-induced tunnelling current flow in atoms, Nat. Phys. **8**, 76 (2012).
[35] S. Popruzhenko and D. Bauer, Strong field approximation for systems with Coulomb interaction, J. Mod. Opt. **55**, 2573 (2008).
[36] S. V. Popruzhenko, G. G. Paulus, and D. Bauer, Coulomb-corrected quantum trajectories in strong-field ionization, Phys. Rev. A **77**, 053409 (2008).
[37] S. Brennecke, N. Eicke, and M. Lein, Gouy's Phase Anomaly in Electron Waves Produced by Strong-Field Ionization, Phys. Rev. Lett. **124**, 153202 (2020).
[38] See Supplemental Material at http://link.aps.org/supplemental/10.1103/PhysRevLett.127.273201 for additional details on the theoretic modeling. In particular, an analytical expression for the initial position from SFA is provided, we show additional electron momentum distributions from modified semiclassical models, and we discuss the angular offsets for different Keldysh parameters, which includes Refs. [6,35,36,39,40].
[39] H. Ni, N. Eicke, C. Ruiz, J. Cai, F. Oppermann, N. I. Shvetsov-Shilovski, and L.-W. Pi, Tunneling criteria and a nonadiabatic term for strong-field ionization, Phys. Rev. A **98**, 013411 (2018).
[40] J. Kaushal and O. Smirnova, Nonadiabatic coulomb effects in strong-field ionization in circularly polarized laser fields, Phys. Rev. A **88**, 013421 (2013).
[41] M. Klaiber, K. Z. Hatsagortsyan, and C. H. Keitel, Tunneling Dynamics in Multiphoton Ionization and Attoclock Calibration, Phys. Rev. Lett. **114**, 083001 (2015).
[42] S. Eckart, M. Kunitski, M. Richter, A. Hartung, J. Rist, F. Trinter, K. Fehre, N. Schlott, K. Henrichs, L. Ph. H. Schmidt, T. Jahnke, M. Schöffler, K. Liu, I. Barth, J. Kaushal, F. Morales, M. Ivanov, O. Smirnova, and R. Dörner, Ultrafast preparation and detection of ring currents in single atoms, Nat. Phys. **14**, 701 (2018).
[43] S. Brennecke, S. Eckart, and M. Lein, Attoclock with bicircular laser fields as a probe of velocity-dependent tunnel-exit positions, J. Phys. B **54**, 164001 (2021).
[44] A. S. Kheifets, The attoclock and the tunneling time debate, J. Phys. B **53**, 072001 (2020).